Macromolecular Research

Article

DOI 10.1007/s13233-018-6086-0

www.springer.com/13233 pISSN 1598-5032 eISSN 2092-7673

Alignment of Cascaded Band-Gap *via* PCBM/ZnO Hybrid Interlayers for Efficient Perovskite Photovoltaic Cells

Soyun Park
Woongsik Jang
Dong Hwan Wang*

School of Integrative Engineering, Chung-Ang University, 84 Heukseok-Ro, Dongjak-gu, Seoul 06974, Korea

Received January 3, 2018 / Revised February 1, 2018 / Accepted February 6, 2018

Abstract: In this study, we investigated methylammonium lead iodide ($MAPbI_3$)-perovskite solar cells (PSCs) with hybrid $PC_{70}BM$/ZnO interlayers. The pristine device which had a $PC_{70}BM$ electron transport layer sandwiched between ITO/PEDOT:PSS/$MAPbI_3$ and TiO_x/Al electrodes exhibited PCE of 12.72% with a V_{OC} of 0.98 V, J_{sc} of 18.41 mA/cm^2, and FF of 71%. The new device with hybrid $PC_{70}BM$/ZnO interlayers exhibited higher PCE of 14.17% with a V_{OC} of 0.98 V, J_{SC} of 20.08 mA/cm^2, and FF of 72% due to the incorporation of ZnO nanoparticles in $PC_{70}BM$ electron transport layer (ETL) with high electron mobility and cascade band gap alignment. Here, we demonstrated that lower photoluminescence (PL) intensity of the device with hybrid interlayers could improve the J_{SC} value of perovskite solar cells due to enhanced charge-generation efficiency. Contact resistance can be reduced by mixing ZnO nanoparticles with $PC_{70}BM$ electron transport layer without additional ZnO layer insertion.

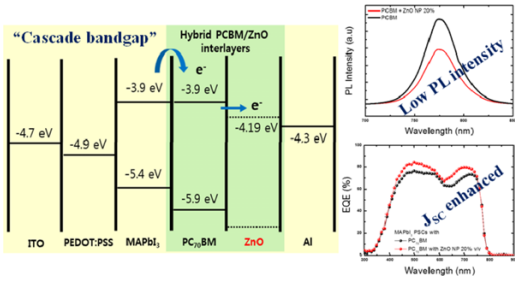

Keywords: ZnO nanoparticles, perovskite solar cells, electron transport layer, hybrid interlayer.

1. Introduction

Organometal halide perovskites, especially the methyammonium lead halide perovskites ($MAPbX_3$, where MA indicates methyammonium and X is the halide), have attracted increasing attention from solar energy harvesters due to high charge-carrier mobility, a direct band gap, a broad absorption range and a long-range exciton diffusion length.[1-6] For about nine years, the power conversion efficiency (PCE) of perovskite solar cells (PSCs) has grown greatly, from the first reported PCE value of 3.8% in 2009 to the recently certified highest value of 22.1%.[7] Therefore, PSCs have two main device structures such as the n-i-p structure and the p-i-n structure. In case of the n-i-p devices, it need to heat at high temperature due to high quality TiO_2 electron transport layer formation which could increase fabrication cost and process stages,[8-12] and hinder using flexible substrates. So, many study of the electron transport layers fabricated at low temperature are recently investigated. In contrast, the p-i-n devices were usually fabricated at much lower temperature, and the low temperature process could be the usage of roll to roll processing. Consequently, many researches on the devices with the p-i-n structure have attracted interest.[13]

The hybrid active layer of polymers doped with inorganic semiconductor nanoparticles has been researched to improve the efficiency of solar cells.[14-17] Especially, many studies have been investigated on doping inorganic nanoparticles in a photoactive layer. These hybrid active layers have the advantage because the inorganic semiconductor materials has high electron mobility. In previous researches, the incorporation of ZnO into P3HT active layer was reasearced.[18-20] The devices with hybrid active layer doped with ZnO nanoparticles enhanced the performance of the organic solar cells, which was attributed to bandgap extraction and to improved electron mobility due to doped ZnO nanoparticles.

In this study, we incorporated ZnO nanoparticles in $PC_{70}BM$ electron transport layers of PSCs and found that such hybrid $PC_{70}BM$/ZnO interlayers resulted in a cascade bandgap alignment. Methods for controlling the interlayer by mixing inorganic nanoparticles could improve electrical properties of perovskite solar cells, resulting in high PCE (%) by increasing short circuit current density (J_{SC}).

2. Experimental

2.1. Materials preparation

For the perovskite layer, methylammonium lead trihaldide (CH_3NH_3I) and lead(II) iodide (PbI_2) at a ratio of 1.06:1 mol·% were dissolved in gamma-butyrolactone (GBL) and dimethyl sulfoxide (DMSO) (7:3 v/v %) at a molar concentration of 1.4 mol/L. The mixture was stirred at 100 °C for 4 h. Clevios P VP AI 4083 type of PEDOT:PSS was purchased from Heraeus (Germany). $PC_{70}BM$ solution was dissolved in chlorobenzene (CB) with a concentration of 20 mg/mL.

2.2. Synthesis of ZnO nanoparticles

ZnO nanoparticles were synthesized according to a modified

Acknowledgments: This research was supported by the Basic Science Research Program through the National Research Foundation of Korea (NRF), funded by the Ministry of Science, ICT & Future Planning (2015M2A2A6A01045277). This research was supported by the Chung-Ang University Research Scholarship Grants in 2016.

***Corresponding Author:** Dong Hwan Wang (king0401@cau.ac.kr)

procedure reported in the literature.[21] Briefly, 0.588 g zinc acetate dihydrate was dissolved in 25 mL methanol with stirring at 60 °C. A solution of KOH in methanol (0.296 g in 13 mL) was then added drop-wise at 60 °C over a period of 12 min. The mixture was stirred at 60 °C for 2 h, resulting in a white ZnO suspension. The suspension was removed from stirring and heating. ZnO precipitate was collected using a centrifuge and washed twice with methanol. After that, CB (20 mg/mL) was added to the precipitate, producing a transparent ZnO nanoparticles dispersion solution. The prepared ZnO nanoparticles solution and $PC_{70}BM$ materials were mixed at a volume ratio of 1:5 and stirred in a glovebox for 6 h.

2.3. Device fabrication

Perovskite solar cells were fabricated on a structure consisting of ITO/PEDOT:PSS/$MAPbI_3$/$PC_{70}BM$(with ZnO NP)/TiO_x/Al as shown in Figure 1(a). To fabricate PSCs, patterned ITO glasses were washed via a 20-min sonication in deionized water, acetone, and 2-propanol. After cleaning, ITO glasses were dried at 100 °C and treated with ultraviolet (UV) ozone for 15 min. PEDOT:PSS solution was spin-coated onto ITO glasses at 5000 rpm for 40 s. PEDOT:PSS films were then annealed on a hot plate at 140 °C for 10 min to generate a thin film with a thickness of 30 nm. $MAPbI_3$ solution was first spin-coated on a PEDOT:PSS film at 1000 rpm for 25 s and immediately spin-coated at 5000 rpm for 30 s with additional process of CB drop-casting. Substrates were then placed on a hot plate at 100 °C for 5 min to fabricate $MAPbI_3$ film with a thickness of 300 nm. The $PC_{70}BM$ layer with a thickness of ~30 nm was spin-coated onto the perovskite layer at 2000 rpm for 40 s. TiO_x interlayer was then added onto the perovskite layer at 5000 rpm for 40 s to generate a thin film with a thickness of ~10 nm. Finally, an Al cathode was thermally deposited under 4.0×10^{-6} Torr with a thickness of ~100 nm using a thermal evaporator. All devices were encapsulated using a UV-curable resin and a cover glass.

2.4. Film characterization

Height image and roughness of the $PC_{70}BM$ ETL and perovskite/$PC_{70}BM$ layers with or without ZnO nanoparticles were characterized using a Park NX10 AFM device (Park Systems, South Korea) in noncontact mode. The size of ZnO nanoparticles was analyzed using a TEM (ARM200F, JEOL, KETI) instrument at 200 kV. In addition, Bruker-AXS XRD device (Bruker, South Korea) was used to investigate the crystallinity of perovskite/$PC_{70}BM$ thin films with or without ZnO nanoparticles.

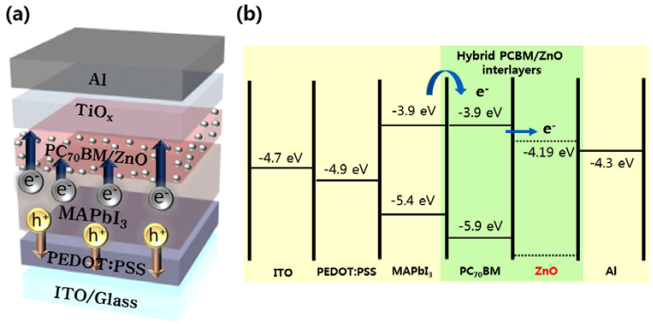

Figure 1. Schematic illustration. (a) Device architecture of perovskite solar cells (PSCs) used in this study, (b) Band diagram of PSCs with hybrid $PC_{70}BM$/ZnO interlayers.

2.5. Device characterization

J-V characteristics of fabricated perovskite solar cells were measured using a ZIVE SP1 instrument (ZIVE LAB, South Korea) under an AM 1.5-G solar simulator and dark conditions. The SCLC was analyzed under light and dark conditions, respectively. Total cell area of PSCs was 0.15 cm^2. External quantum efficiency (EQE) (%) values were measured to prove short-circuit current (J_{SC}). PL spectra were measured using an XPERAM 200 Raman microscope (Nanobase, Inc., South Korea) with laser wavelength of 642 nm and power of 0.3 mW for each device.

3. Results and discussion

The performances of perovskite photovoltaic devices were highly dependent on the incorporation of ZnO nanoparticles into the $PC_{70}BM$ electron transport layer. We, therefore, fabricated the devices with 0~40% v/v of ZnO nanoparticles into $PC_{70}BM$ in order to confirm the effect of ratio dependence related $PC_{70}BM$ (See in Table S1 and Figure S1). As a results, the device with 5% v/v ZnO nanoparticles in $PC_{70}BM$ exhibits less effective, and also the devices with 30~40% v/v of ZnO nanoparticles show a decreased efficiency due to un-optimized concentration from the excess ZnO nanoparticles. Consequently, we confirmed the proper ZnO nanoparticles ratio at 20% v/v in $PC_{70}BM$ based on the results from electrical parameters and external quantum efficiency (EQE) (%) of the device. For the pristine cell, the perovskite solar cell with a $PC_{70}BM$ interlayer exhibited an efficiency as high as 12.72%. When the hybrid $PC_{70}BM$/ZnO interlayers were used, FF was slightly increased. The hybrid $PC_{70}BM$/ZnO interlayers could enhance the generated electron transportation to cathode due to the high electron mobility of ZnO nanoparticles in the interlayer and cascade bandgap alignment by applying the hybrid $PC_{70}BM$/ZnO interlayers as shown in Figure 1(b).[20] After ZnO nanoparticles were doped, the PCE of the device with hybrid $PC_{70}BM$/ZnO interlayers was increased up to 10% compared to the device with pristine $PC_{70}BM$. Furthermore, the combination process such as $PC_{70}BM$ with ZnO nanoparticles resulted in optimum device parameters, including power conversion efficiency (PCE) of 14.17% with an open circuit voltage (V_{OC}) of 0.98 V, short circuit current (J_{SC}) of 20.08 mA/cm^2, and fill factor (FF) of 72% (Figure 2(a) and Table 1). The EQE and *J-V* curves in the dark of Figure 2(b), and 2(c) are correlated with those show in Figure 2(a), respectively. In general, the FF increased when series resistance (R_s) decreased as shown in Figure 2(c). R_s could be attributed to Ohmic loss in the whole device which included bulk resistance and contact resistance. Therefore, R_s was affected not only by the resistivity of the pristine $PC_{70}BM$ layer and the hybrid $PC_{70}BM$/ZnO interlayers, but also by other factors such as contact resistance between different layers. The improvement in photocurrent due to applying ZnO nanoparticles was consistent with EQE measurement. EQE showed an improvement in

Table 1. Photovoltaic parameters of perovskite solar cells (PSCs) devices fabricated with or without hybrid $PC_{70}BM$/ZnO interlayers depending on current density–voltage (*J–V*) curve

Electron transport layer	V_{OC} (V)	J_{SC} (mA/cm^2)	EQE (mA/cm^2)	FF (%)	PCE (%)
Only $PC_{70}BM$	0.98	18.41	16.96	0.71	12.72
The hybrid $PC_{70}BM$/ZnO interlayers	0.98	20.08	18.38	0.72	14.17

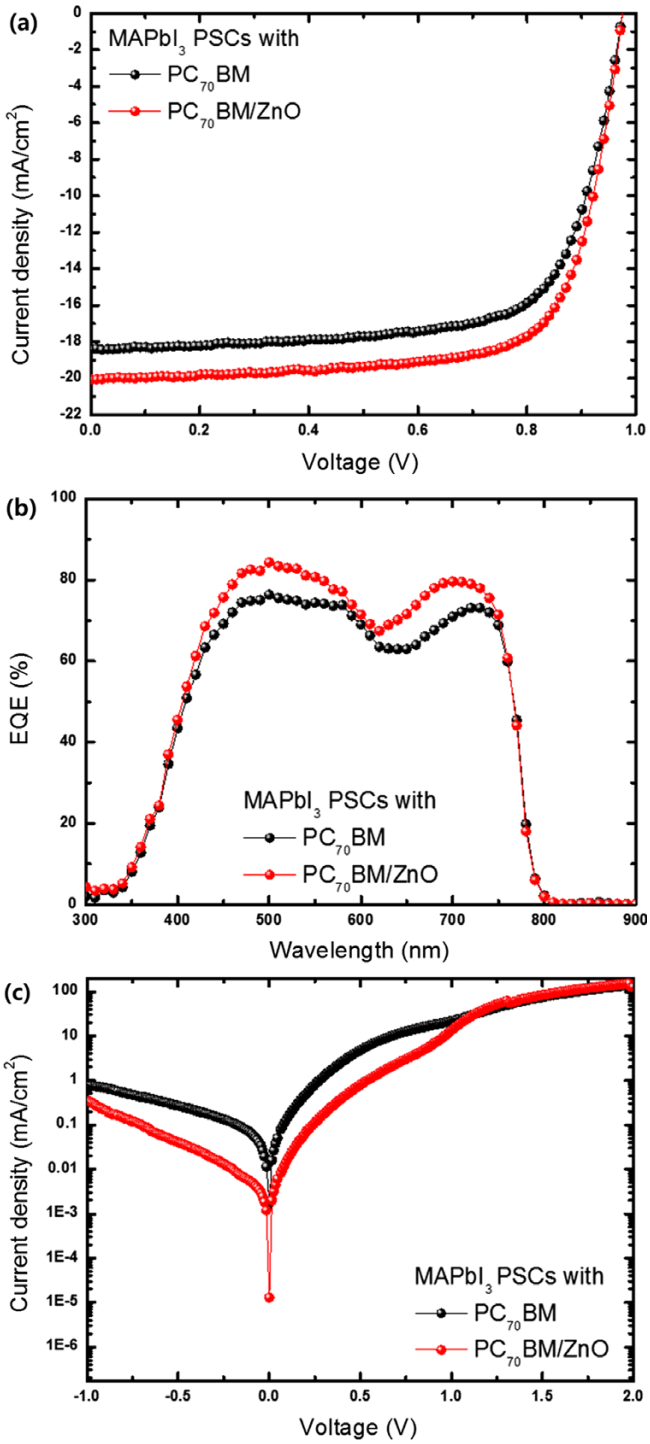

Figure 2. (a) Current-voltage (*J-V*) characteristics of perovskite solar cells (PSCs) fabricated with or without hybrid $PC_{70}BM$/ZnO interlayers under AM 1.5-G irradiation at 100 mW/cm^2. (b) External quantum efficiency (EQE) (%) of PSCs depending on *J-V* characteristics. (c) Dark current-voltage characteristics of perovskite solar cells (PSCs) fabricated with or without hybrid $PC_{70}BM$/ZnO interlayers under dark.

current density for the entire wavelength range from 400 nm to 750 nm. EQE values for devices doped with ZnO nanoparticles were increased, resulting in the highest J_{SC} value as shown in Figure 2(b). Thus, EQE improvements could be explained as the effect of hybrid $PC_{70}BM$/ZnO interlayers in the perovskite solar cell. As seen in Figure 2(c), the perovskite device with hybrid $PC_{70}BM$/ZnO interlayers exhibited the lower R_s and larger shunt resistance (R_{sh}) compared to the only $PC_{70}BM$, meaning that the resistance for carrier transport in the device was minimized and carrier loss through recombination was effectively blocked, leading to an improvement in J_{SC} and FF.[22,23]

As shown in Figure S2, electron-only devices with ITO/PEI/$MAPbI_3$/$PC_{70}BM$(with ZnO)/TiO_x/Al structure were fabricated to measure electron mobility using space-charge limited current (SCLC).[24] PSCs with hybrid $PC_{70}BM$/ZnO interlayers resulted in enhanced electron mobility. Thus, we could consider that hybrid $PC_{70}BM$/ZnO interlayers could lead to both electron mobility and excellent electron transportation. The role of ZnO nanoparticles increased solar cell performance compared to pristine perovskite solar cells. Hybrid $PC_{70}BM$/ZnO interlayers were crucial for improving the performance of solar cell devices with high J_{SC} values as shown in Figure 2(a)-(c). It is clear that the interlayer doped with ZnO nanoparticles can increase the J_{SC} value of cells due to its low resistivity. In this result, perovskite solar cells could improve the J_{SC} value because the contact resistance can be reduced by mixing ZnO nanoparticles with $PC_{70}BM$ electron transport layer without additional ZnO layer insertion.[25] Transmission electron microscope (TEM) images of ZnO nanoparticles

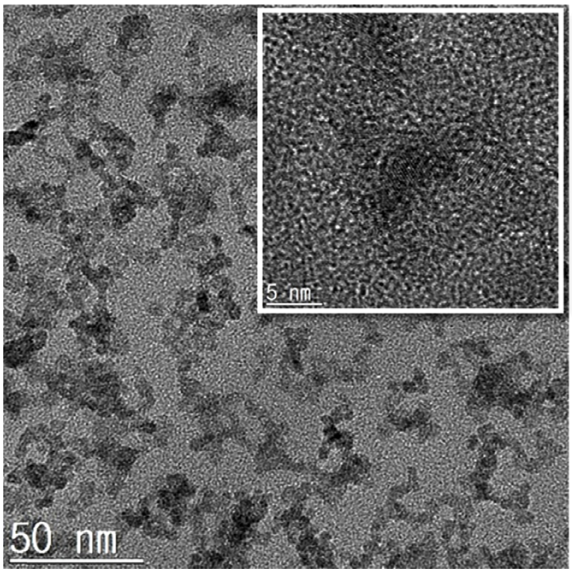

Figure 3. Transmission electron microscope (TEM) images of synthesized ZnO nanoparticles spin-coated on the indium tin oxide (ITO) glass with insertion of magnified images.

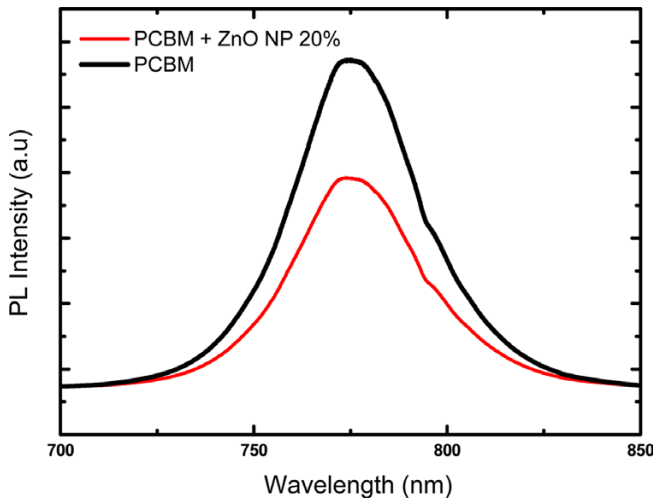

Figure 4. Photoluminescence (PL) spectra of $PC_{70}BM$ with or without hybrid $PC_{70}BM$/ZnO interlayers on the top of the $MAPbI_3$ layer measured at laser wavelength of 642 nm and power of 0.3 mW.

were prepared. Figure 3 shows narrow size distribution and low tendency towards aggregation of these nanoparticles. An average size of these nanoparticles was estimated to be 5 nm using TEM as displayed in the inset.

On contact with charge transport layers, perovskite films typically exhibited strong photoluminescence (PL) quenching as evidence of efficient charge transfer from the photoactive layer to the transport layer. Figure 4 shows photoluminescence of ITO/PEDOT:PSS/perovskite/$PC_{70}BM$ and ITO/PEDOT:PSS/perovskite/$PC_{70}BM$ with ZnO. Reduced PL intensity associated with efficient charge separation or injection from the photoactive material to the charge-extraction layer was observed for the hybrid $PC_{70}BM$/ZnO interlayers. As a result, the hybrid $PC_{70}BM$/ZnO interlayers on the perovskite layer exhibited a decreased PL intensity. This was attributed to the significant J_{SC} increase in the functioning PSCs device. Therefore, it could be worthwhile to highlight that the hybrid $PC_{70}BM$/ZnO interlayers is subjected to more efficient dissociation of excitons into free charge carriers compared to the Only-$PC_{70}BM$ layer, leading to improved charge-generation efficiency.

X-Ray diffraction (XRD) was performed to analyze the change in perovskite crystallinity according to hybrid $PC_{70}BM$/ZnO interlayers (Figure 5). Five diffraction peaks of the pristine $PC_{70}BM$ on perovskite layer could be clearly observed. We can clearly show that the diffraction peaks of $MAPbI_3$ with the pristine $PC_{70}BM$ and the hybrid $PC_{70}BM$/ZnO interlayers are almost similar results, as both exhibit strong diffraction peaks located at 14.11° and 28.41°, which could be assigned to the (110) and (220) planes of $MAPbI_3$ (See in Figure 5).[26] This phenomenon indicated that hybrid $PC_{70}BM$/ZnO interlayers were coated onto the perovskite thin film with a uniformed surface coverage. Therefore, the hybrid $PC_{70}BM$/ZnO interlayers played an important role in the increase of J_{SC} in the device. This is associated with the hole-blocking nature of ZnO with enhanced carrier selectivity and uniform surface coverage of $PC_{70}BM$ layer which can contribute to the preserved crystalline structure of $MAPbI_3$ from the role of ETL.[25,27]

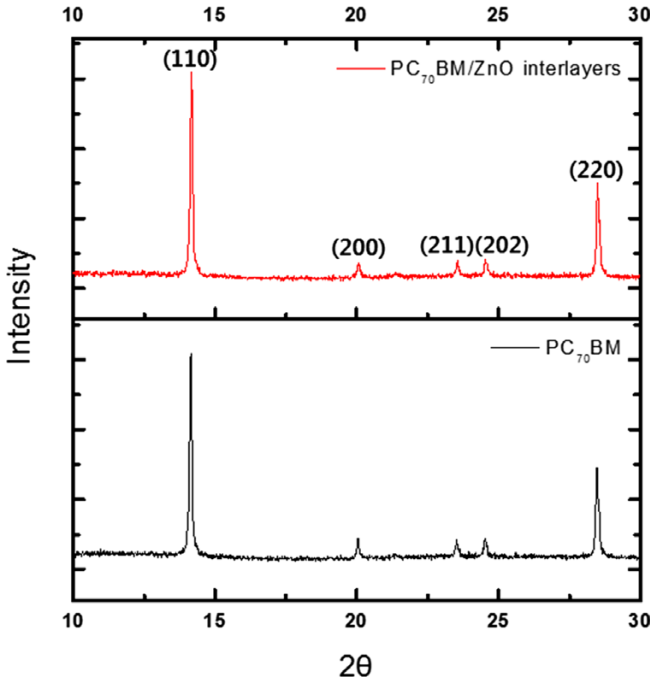

Figure 5. X-Ray diffraction (XRD) profiles of pristine $PC_{70}BM$ and hybrid $PC_{70}BM$/ZnO interlayers on perovskite layers.

Atomic force microscopy (AFM) was used to characterize pristine $PC_{70}BM$ and $MAPbI_3$/$PC_{70}BM$ films compared to $PC_{70}BM$ doped with ZnO nanoparticles and $MAPbI_3$/$PC_{70}BM$ doped with ZnO nanoparticles films. All images within a surface area of 5 μm×5 μm were collected as shown in Figure 6. Height morphologies of pristine $PC_{70}BM$ and the $PC_{70}BM$ doped with ZnO nanoparticles on the ITO were similar. $PC_{70}BM$ doped with ZnO nanoparticles film showed an even surface similar to pristine

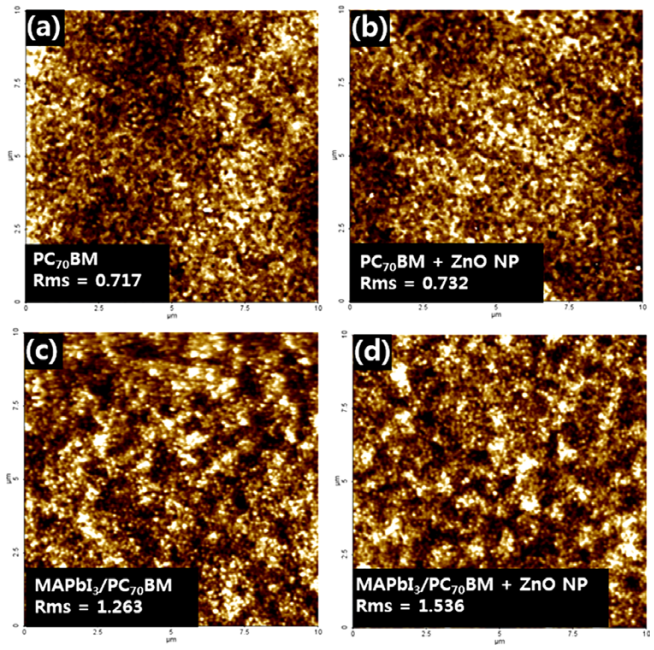

Figure 6. Atomic force microscopy (AFM) height images of films with 5 μm×5 μm dimensions according to each layer. (a) ITO/$PC_{70}BM$ film, (b) ITO/the hybrid $PC_{70}BM$/ZnO interlayers, (c) ITO/$MAPbI_3$/$PC_{70}BM$, and (d) ITO/$MAPbI_3$/the hybrid $PC_{70}BM$/ZnO interlayers.

$PC_{70}BM$ film. Their root mean square (RMS) roughness values were 0.73 nm and 0.72 nm, respectively. Therefore, the difference in RMS-roughness value between the two was very small, clearly demonstrating that the surface roughness of $PC_{70}BM$ doped with ZnO nanoparticles coating on top of the $MAPbI_3$ exhibited a stable surface even though ZnO nanoparticles were doped. Thus, AFM height morphologies clearly revealed that addition of ZnO nanoparticles into the electron transport layer slightly increased the roughness of films. RMS roughness of pristine $MAPbI_3/PC_{70}BM$ layer was 1.26 nm. That of $PC_{70}BM$/ZnO interlayers was 1.53 nm.[28] When ZnO nanoparticles were contained in the $PC_{70}BM$ layer, the surface was rougher than that of the pristine $PC_{70}BM$ layer due to adding 5 nm size of ZnO nanoparticles. Such roughness of $PC_{70}BM$ doped with ZnO nanoparticles layer could result in greater light absorption due to diffuse reflection between $MAPbI_3/PC_{70}BM$ layers and top electrode.[29]

4. Conclusions

In summary, utilizing the advantage of hybrid $PC_{70}BM$/ZnO interlayers, we can fabricate $MAPbI_3$ based perovskite solar cells with increased efficiency of over 10% compared to device with pristine $PC_{70}BM$ layer. $PC_{70}BM$ ETL containing ZnO nanoparticles exhibited increased J_{SC} values of perovskite solar cells. Both electron mobility and excellent electron transportation of ZnO resulted in increased J_{SC} values of PSCs. Therefore, ZnO nanoparticles not only affected energy band gap alignment such as a cascade arrangement, but also had hole-blocking nature. Thus, devices associated with ZnO nanoparticles showed enhanced carrier selectivity and uniform surface coverage of hybrid $PC_{70}BM$/ZnO interlayers confirmed by PL analysis and AFM height images, respectively. Taken together, these results give us a guideline for further electron transport layer development of perovskite solar cells where both long-term stability and band gap alignment should be studied for high performance PSCs fabrication.

Supporting information: Information is available regarding the electrical parameters of PSCs with hybrid interlayers from 0~40% ratio of ZnO nanoparticles and analysis of electron mobility depending on device with ZnO nanoparticles. The materials are available *via* the Internet at http://www.springer.com/13233.

References

(1) J. Burschka, N. Pellet, S. J. Moon, R. Humphry-Baker, P. Gao, M. K. Nazeeruddin, and M. Grätzel, *Nature*, **499**, 316 (2013).
(2) M. M. Lee, J. Teuscher, T. Miyasaka, T. N. Murakami, and H. J. Snaith, *Science*, **338**, 643 (2012).
(3) J. H. Heo, S. H. Im, J. H. Noh, T. N. Mandal, C. S. Lim, J. A. Chang, and M. Grätzel, *Nat. Photonics*, **7**, 486 (2013).
(4) S. D. Stranks, G. E. Eperon, G. Grancini, C. Menelaou, M. J. Alcocer, T. Leijtens, and H. J. Snaith, *Science*, **342**, 341 (2013).
(5) G. E. Eperon, S. D. Stranks, C. Menelaou, M. B. Johnston, L. M. Herz, and H. J. Snaith, *Energy Environ. Sci.*, **7**, 982 (2014).
(6) S. Ahn, W. Jang, S. Park, and D. H. Wang, *ACS Appl. Mater. Interfaces*, **9**, 15623 (2017).
(7) D. Bi, C. Yi, J. Luo, J. D. Décoppet, F. Zhang, S. M. Zakeeruddin, and M. Grätzel, *Nature Energy*, **1**, 16142 (2016).
(8) A. Kojima, K. Teshima, Y. Shirai, and T. Miyasaka, *J. Am. Chem. Soc.*, **131**, 6050 (2009).
(9) N. J. Jeon, J. H. Noh, Y. C. Kim, W. S. Yang, S. Ryu, and S. Il. Seok, *Nat. Mater.*, **13**, 1 (2014).
(10) H. S. Kim, C. R. Lee, J. H. Im, K. B. Lee, T. Moehl, A. Marchioro, S. J. Moon, R. Humphry-Baker, J. H. Yum, J. E. Moser, M. Grätzel, and N. G. Park, *Sci. Rep.*, **2**, 591 (2012).
(11) J. H. Noh, N. J. Jeon, Y. C. Choi, M. K. Nazeeruddin, M. Grätzel, and S. I. Seok, *J. Mater. Chem. A*, **1**, 11842 (2013).
(12) S. Ryu, J. H. Noh, N. J. Jeon, Y. C. Kim, W. S. Yang, J. Seo, and S. I. Seok, *Energy Environ. Sci.*, **7**, 2614 (2014).
(13) J. You, Z. Hong, Y. M. Yang, Q. Chen, M. Cai, T. B. Song, and Y. Yang, *ACS Nano*, **8**, 1674 (2014).
(14) J. D. Olson, G. P. Gray, and S. A. Carter, *Sol. Energy Mater. Sol. Cells*, **93**, 519 (2009).
(15) N. Zhao, T. P. Osedach, L. Y. Chang, S. M. Geyer, D. Wanger, M. T. Binda, and V. Bulovic, *ACS Nano*, **4**, 3743 (2010).
(16) N. Radychev, I. Lokteva, F. Witt, J. Kolny-Olesiak, H. Borchert, and J. Parisi, *J. Phys. Chem. C*, **115**, 14111 (2011).
(17) D. Yun, W. Feng, H. Wu, and K. Yoshino, *Sol. Energy Mater. Sol. Cells*, **93**, 1208 (2009).
(18) M. Wang and X. Wang, *Sol. Energy Mater. Sol. Cells*, **92**, 766 (2008).
(19) W. J. Beek, M. M. Wienk, and R. A. Janssen, *Adv. Funct. Mater.*, **16**, 1112 (2006).
(20) S. H. Oh, S. J. Heo, J. S. Yang, and H. J. Kim, *ACS Appl. Mater. Interfaces*, **5**, 11530 (2013).
(21) D. Liu and T. L. Kelly, *Nat. Photonics*, **8**, 133 (2013).
(22) R. Casalini, S. W. Tsang, J. J. Deininger, F. A. Arroyave, J. R. Reynolds, and F. So, *J. Phys. Chem. C*, **117**, 13798 (2013).
(23) S. R. Cowan, R. A. Street, S. Cho, and A. J. Heeger, *Phys. Rev. B*, **83**, 035205 (2011).
(24) J. Kim, G. Kim, H. Back, J. Kong, I. W. Hwang, T. K. Kim, S. Kwon, J. H. Lee, J. Lee, K. Yu, C. L. Lee, H. Kang, and K. Lee, *Adv. Mater.*, **28**, 3159 (2016).
(25) H. L. Yip and A. K. Y. Jen, *Energy Environ. Sci.*, **5**, 5994 (2012).
(26) X. Zeng, T. Zhou, C. Leng, Z. Zang, M. Wang, W. Hu, and M. Zhou, *J. Mater. Chem. A*, **5**, 17499 (2017).
(27) S. Chen, J. R. Manders, S. W. Tsang, and F. So, *J. Mater. Chem.*, **22**, 24202 (2012).
(28) Y. Shao, Z. Xiao, C. Bi, Y. Yuan, and J. Huang, *Nat. Commun.*, **5**, 5784 (2014).
(29) W. Qiu, M. Buffière, G. Brammertz, U. W. Paetzold, L. Froyen, P. Heremans, and D. Cheyns, *Org. Electron.*, **26**, 30 (2015).